

Earth and Space Science



TECHNICAL REPORTS: METHODS

10.1029/2020EA001575

Key Points:

- DC electrical resistivity meter
- Modular device
- Open-source electronic platform

Correspondence to:

M. V. Bongiovanni,
mbongiovanni@austral.edu.ar

Citation:

de la Vega, M., Bongiovanni, M. V., & Grünhut, V. (2021). Design of a low-cost electrical resistivity meter for near surface surveys. *Earth and Space Science*, 8, e2020EA001575. <https://doi.org/10.1029/2020EA001575>



Received 21 NOV 2020

Accepted 19 NOV 2021

Author Contributions:

Conceptualization: M.de la Vega
Data curation: M. V. Bongiovanni, V. Grünhut
Formal analysis: M.de la Vega
Investigation: M.de la Vega
Methodology: M. V. Bongiovanni
Project Administration: M.de la Vega
Software: V. Grünhut
Supervision: M.de la Vega
Validation: M.de la Vega
Visualization: M. V. Bongiovanni
Writing – original draft: M. V. Bongiovanni

Design of a Low-Cost Electrical Resistivity Meter for Near Surface Surveys

M. de la Vega¹, M. V. Bongiovanni² , and V. Grünhut² 

¹GAIA (Grupo de Geofísica Aplicada y Ambiental), Buenos Aires University, IFIBA-CONICET, Buenos Aires, Argentina,

²LIDTUA, Facultad de Ingeniería, Universidad Austral, and CONICET, Buenos Aires, Argentina

Abstract A programmable automated electrical resistivity meter was designed and constructed. The device was created to perform near surface studies, particularly for archaeogeophysical target characterization. Real field and laboratory model studies can be performed changing the current input of the device. The equipment consists of two independent devices, each one with its own microcontroller platform. They are interconnected through serial data transfer protocol. The first device, works as a resistivity meter where the ABMN electrode positions are programmed and permits the interaction with the user. The second one, connects the current and voltage channels to the programmed electrode positions. A physical model and field measurements were performed with different electrode configurations such as Dipole-Dipole, Werner-Schlumberger and Wenner γ_{112} in order to verify the performance of the automated electrical resistivity meter. The measurements give mean relative standard deviation values between 0.6% and 5.5% and data inversion convergence between 1.3% and 7.2%. Even though this open source and low cost electrical resistivity meter was design primarily for archaeogeophysical studies, it could be adapted to other geophysical issues such as contamination plumes detection and characterization, tunnel detection, etc.

1. Introduction

The direct current electrical resistivity technique is one of the most reliable geophysical prospection methods (Dahlin, 1996). With this method, surface voltage differences produced by current flow in earth provide accurate information about the resistivity distribution in the subsurface (Stummer et al., 2004). 2D and 3D imaging obtained with this method is commonly used in different study areas: urban environmental prospection (Chávez et al., 2014; Eleraki et al., 2010; Tsokas et al., 2011), tunnel detection (Bongiovanni et al., 2018; Orfanos & Apostolopoulos, 2011; Osella et al., 2015; Simyrdanis et al., 2015), as an aid of archeological studies (Casas et al., 2018; Tejero-Andrade et al., 2018), civil engineering studies (Gutiérrez-Martín et al., 2021; Himi et al., 2018; Santarato et al., 2011), contaminant plumes characterization (Chambers et al., 2006; Vaudelet et al., 2011), surface-down-hole measurements (Bergmann et al., 2012; Clément et al., 2014; Ochs & Klitzsch, 2020), earthquakes and geological hazards (Saribudak & Van Nieuwenhuise, 2006; Kamiński et al., 2021), aquifer characterization (Fowler & Moysey, 2011; Froese et al., 2005; Sendrós et al., 2020; Yeh et al., 2015), etc.

With the development of faster hardware and more efficient software, the increasingly number of data involved can be easily managed. Also, survey strategies can be modified interactively (Wilkinson et al., 2006). With these advances, reliable electrical resistivity tomographies are obtained of the studied targets or sites.

Commercial and non-commercial resistivity automated multielectrode systems are basically of two types: centralized and distributed (Bulgakov & Manshtein, 2006; Kutbay & Hardalaç, 2017; Stummer et al., 2002; Zhe et al., 2007). In the centralized systems, a unique controller through multiplexors open the different channels for current flow and voltage measurements. In the distributed systems, each electrode has the electronic components required for the measurements.

We developed a programmable automated resistivity meter, whose system is centralized. It was designed to study near surface geophysical targets in the field and on laboratory scale, which has required to handle two different current and voltage scales. The equipment was built in such a way that modules can be added, for example, allowing data transfer to the web or including a GPS module for geolocalization. Another factor that we took into account in the design is that it can be extended with modules to handle additional number of electrodes as needed. A first version of the device has been reported by de la Vega et al. (2019).

© 2021 The Authors. Earth and Space Science published by Wiley Periodicals LLC on behalf of American Geophysical Union.

This is an open access article under the terms of the [Creative Commons Attribution License](https://creativecommons.org/licenses/by/4.0/), which permits use, distribution and reproduction in any medium, provided the original work is properly cited.

From the first years of the current century open source platforms are available that have been used for both basic and applied research (Mao et al., 2019). This coincides with the development of microcontroller platforms such as Arduino products (<https://www.arduino.cc/>) and single-board computers like the Raspberry Pi (<https://www.raspberrypi.org/>). This type of equipment allows to customize the application and to use adaptive monitoring or feedback and real-time control. Another advantage of these types of developments is that they enable a wide range of possibilities for user interaction. Sensor data can be transmitted from network-based data loggers to a web-based data exchange portal (Horsburgh et al., 2019). Equipment developed in this type of platform for environmental studies include for example, CO₂ monitoring (Blackstock et al., 2019) and water monitoring (Tziortzioti et al., 2019).

A centralized system is developed using an open-source electronic platform. The design and construction were performed taking into account Arduino platform capabilities. This platform, has a complete set of compatible modules to perform the different tasks of the device.

Different parts/functions of the device are managed by different processors interconnected via serial connection. The cables used are conventional. The electrodes, of galvanic contact, have no special design and multiple voltage measurements can be done with a single current shot for any electrode configuration via programming.

One of the advantages of the present device over the commercially available ones is that the high cost of them make difficult to acquire in developing countries. In other cases, the low cost and relatively simple construction of the present device enable to have it as a second tool, allowing the immobilization of the device for several days, for 4D monitoring of waste dumps (Clement et al., 2011), landslides (Wilkinson et al., 2016), saltwater intrusion in coastal aquifers (Kuras et al., 2009), monitoring of soil moisture dynamics (Chambers et al., 2014) among the most significant applications.

In the following sections we first describe the modular electrical resistivity meter developed. Next, we present the laboratory test and the field measurements performed in order to verify its performance. We show the inversion results with different electrode configurations. Finally, the conclusions of the work carried out are exposed.

2. Electrical Resistivity Meter Design and Construction

The electrical resistivity meter was designed in two independent hardware modules, each one with its own main-frame interconnected via serial protocol. In both units an Arduino Mega 2560 (ATmega2560 microcontroller) is used as the processing unit. It has a cpu clock of 16 Mhz, 54 digital input/output pins with 5 V logic and supports I2C and SPI as well as four serial facilities for communication with other devices. As power supply we used a commercial inverter of 220 V powered by a 12 V battery, whose signal was rectified by a diode bridge. It provides several output voltages: 100, 75, 50, 25 and 12 V.

The first device, the driver, is the main one. It works like a common electrical resistivity meter. It also points out to the second device, the automated platform, the electrode to be connected. The automated platform acts as an intelligent relay matrix system that connects the different current and voltage channels to the electrodes where current is injected and voltage is measured.

The microcontroller of the driver device performs three different types of operations. The main function is to perform the current and voltage measurements. The second function is to control the different components that allow the user-device interaction. The third one is to send an order to the automated device with the information of which electrodes should be connected to the different current and voltage channels. Figure 1 shows the block diagram of the electrical resistivity meter.

The current is measured with the Arduino compatible sensor INA 219 (I in Figure 1 -channels A and B-) via the I2C bus. This sensor uses a shunt resistance of 0.1 ohm combined with a 12 bits analog digital converter (ADC). It can measure current between ± 3.2 A with a resolution of 0.8 mA. Also it has a programmable gain amplifier (PGA) that can be programmed, for example, to measure currents between ± 400 mA with a resolution of 0.1 mA. To the current circuit we attach a interchangeable limiting resistance (R) to be used with different current scales and a relay (Re) to start the current flow.

The voltage is measured with the analog digital converter ADS 1115 (V in Figure 1 -channels M1, N1, M2 and N2-) that connects via the I2C bus. This board has a resolution of 16 bits (15 bits for the magnitude and one bit

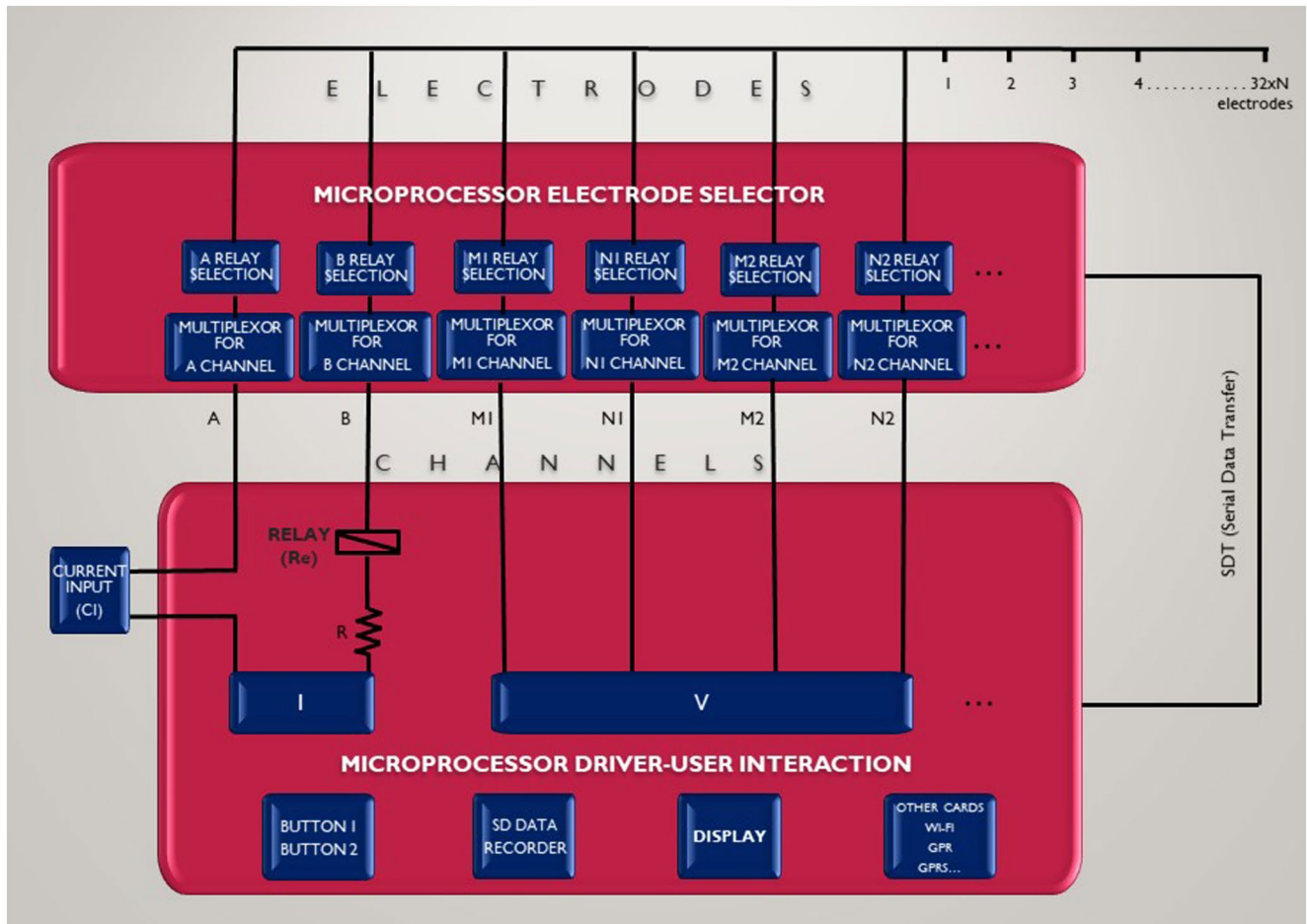


Figure 1. Block diagram of the electrical resistivity meter. Blue blocks are modules attached to the processors.

for the sign) and four channels which can be configured as two differential sensors. Four boards can be connected, using different addresses, configuring a system of eight differential channels. The voltage range of ADS1115 is ± 6.144 V. The resolution for this range is 0.1875 mV. With the incorporated PGA set to gain one, the voltage range is ± 4.096 V with 0.125 mV resolution.

The current source is external to the device (CI in Figure 1). This current is adapted to the characteristic of the study to be made. The voltage and current ranges are modified by software while the limiting resistance is modified by hardware. Their values depend on the type of study we perform. For example, for near surface studies, we could use 50 V as input with a limiting resistance of 100 ohm, hence a maximum current of 0.5 A can be obtained. For physical model studies we use 12 V and 560 ohm limiting resistance, therefore a maximum current of 0.02 A is obtained. In both cases the current input is a square wave of period 200 ms, and V and I are sampled with a frequency of 100 samples/second. For each ABMN electrodes position five shots are made. This parameters are controlled by software that can be modified as needed.

In the first device, that commands the user-driver interaction, both the injection (A, B) and the voltage (M1, N1 M2, N2, etc.) electrodes positions are programmed. These configurations are programmed in the EEPROM memory of the microprocessor (4,096 bytes available on Arduino Mega).

The user-device interfaces we implement to manage the equipment are: a SD card to record the data obtained, a LCD display to visually see the status of the equipment and a couple of buttons to select/start processes. Different electrode configurations kept in memory are selected via these buttons.

The automated device redirects the channels connected to the driver device to the appropriate electrodes. The information of the electrodes positions is obtained from the driver by serial transmission. Each channel is connected

Table 1
Example of Input - Output Data

Input data				Output data		
A	B	M1	N1	Measurement	$\Delta V/I$	I
0	1	2	3	1	14.42	10.10
				1	14.24	10.40
				1	14.53	10.30
				1	14.22	10.30
				1	14.45	10.30
0	1	3	4	2	4.11	10.30
				2	4.00	10.30
				2	3.95	10.30
				2	3.88	10.30
				2	4.01	10.30
0	1	4	5	3	1.50	10.50
				3	1.38	10.30
				3	1.37	10.30
				3	1.41	10.50
				3	1.49	10.50
0	1	5	6	4	0.75	10.30
				4	0.61	10.10
				4	0.56	10.30
				4	0.67	10.30
				4	0.71	10.30
–	–	–	–	–	–	–
–	–	–	–	–	–	–
–	–	–	–	–	–	–
19	23	27	31	212	4.77	9.20

in the automated device to a multiplexor/demultiplexor (74HC4067) Arduino compatible module. Each multiplexor in turn is connected to a 16 relay board. This processor, once the electrodes positions received, indicates to each multiplexor which relay (electrode) has to be connected. In the constructed automated device each channel is connected to two multiplexor/relay board so 32 electrodes are available. This can be upgraded up to 256 electrodes. The electrodes are attached to the automated device using standard cables.

The overall operation of the system is as follows. After a setup protocol of both the Driver device microprocessor and the Automated device microprocessor, the user is asked to select one of the electrode configuration kept in the Driver's memory. The electrodes positions are send to the Automated device, which in turn connects the channels to the selected electrodes. After the Driver performs the apparent electrical resistivity measurements, the resulting data is send to memory and the next electrodes positions are send to the Automated. The loop continues until the last electrode position is measured and the data is saved in the SD card.

An example of the electrode position and output of the device is shown in Table 1. The first four columns show the position of the electrodes corresponding to a dipole-dipole configuration in the EEPROM memory of the Driver. Only one voltage measurement per current input (channel M1-N1) is programmed in this example. The last three columns show the output of the device kept in the SD card. Five measurements are made for each position of the electrodes.

Table 2
Configurations Programmed in the Device

Array	Measurements	N_{\max}	A	Electrode distribution
D-D	106	6	1,2,3,4	A-a-B-na-M-a-N
W-S	80	6	1,2,3	A-na-M-a-N-nB
$W\gamma_{112}$	48		1,2,3,4,5	A-a-M-a-B-2a-N N-2a-B-a-M-a-A

3. Performance of the Device

In order to evaluate the performance of the constructed device we performed a target detection and characterization studies in a physical model and in the field.

3.1. Sphere Target Detection Study

We studied a sphere submerged in salt water. We performed 2D tomographies of it using in-line Dipole-Dipole, Wenner-Schlumberger, and Wenner γ_{112} (plus mirror) configurations. This last electrode configuration was included

due to its efficiency to characterize localized targets with few measurements (Szalai et al., 2015). We have programmed the electrode positions as shown in Table 2. We also performed 3D measurements using Dipole-Dipole configuration.

The target studied was submerged in a plastic container filled with saltwater of horizontal dimensions 35×25 cm and 12 cm height, and was placed in a region of dimensions 15×215 cm in the central part of the box to eliminate boundary contributions. The diameter of the sphere was of 3 cm, it was submerged at 1 cm from the top surface, and centered in the horizontal plane. As the resolution obtained with the geoelectric method is about half the electrode separation, 16 electrodes 1 cm apart were used. In Figure 2a can be seen a photo of the physical model and the device prepared for the sphere study.

To prevent electrolysis effects a low current input was used. This is generated using 12V input and a limiting resistance of 560 ohm then a maximum current of 0.02 A is achieved.

For this configuration, the voltage ADC PGA is set to gain one: the voltage range is ± 4.096 V with 0.125 mV resolution. The current PGA is programmed to measure currents between ± 400 mA with a resolution of 0.1 mA. The device was programmed to take five measurements in each A, B, M1, N1 position (only one differential voltage was measured at a time) and record the time evolution of voltage/current at each A B M1 N1 positions.

An example of the time evolution of an individual measurement made in the physical model is shown in Figure 2b. A Dipole-Dipole configuration was taken with $a = 1$ cm and $n = 3$. From this graph, we obtain a $\Delta V/I$ mean value of 1.563 ohm and relative standard deviation of 0.6%. The physical model tomographies give similar results over all relative standard deviation of the $\Delta V/I$ data obtained.

The mean relative standard deviation of the 106 Dipole-Dipole measurements is 3.8%, with a minimum of 0.2% and a maximum of 37%. For the 80 Wenner-Schlumberger measurements the values are, mean: 0.7%, minimum: 0.2% and maximum: 1.4%. The values for the 48 $W\gamma_{112}$ and mirror measurements are, mean: 3.9%, minimum: 0.4% and maximum: 39.9%. The highest error of measurements values comes from the furthest potential electrodes, that corresponds to the values of the lower voltage differences. These few points were eliminated before doing the inversion process. In the Schlumberger-Wenner case, the dispersion was less because the potential electrodes are between the current ones.

In Figure 3 we can see the inversion results of the configurations mentioned above. They were performed using the RES2DINV code (Loke & D Barker, 1996). The quality of the inversion of ERT data was determined by the value of the RRMS (Relative Root Mean Square). In all the cases, for the interpretation we choose the model for which the inversion achieved an acceptable absolute error.

Figure 3a shows the results of the D-D configuration. The high electrical resistivity ball can be distinguished, and the convergence is very good; that is, the RRMS deviation was 1.31%. Figure 3b shows the results of the W-S configuration. The ball can be distinguished and the convergence is very good (RRMS 1.75%). Figure 3c shows the results of $W\gamma_{112}$ configuration. The convergence is also good (RRMS 7.2%), the ball can be perfectly distinguished and the resolution was very good.

We also performed 3D measurements in the container using the same sphere but with the medium less conductive than in the previous case. The sphere was submerged at 1 cm from the saltwater top surface and centered in the horizontal plane. We performed sixteen dipole-dipole profiles along X axis every 1 cm, and six profiles along Y axis separated 3 cm. In each profile, sixteen electrodes were used with 1 cm separation between them. The data

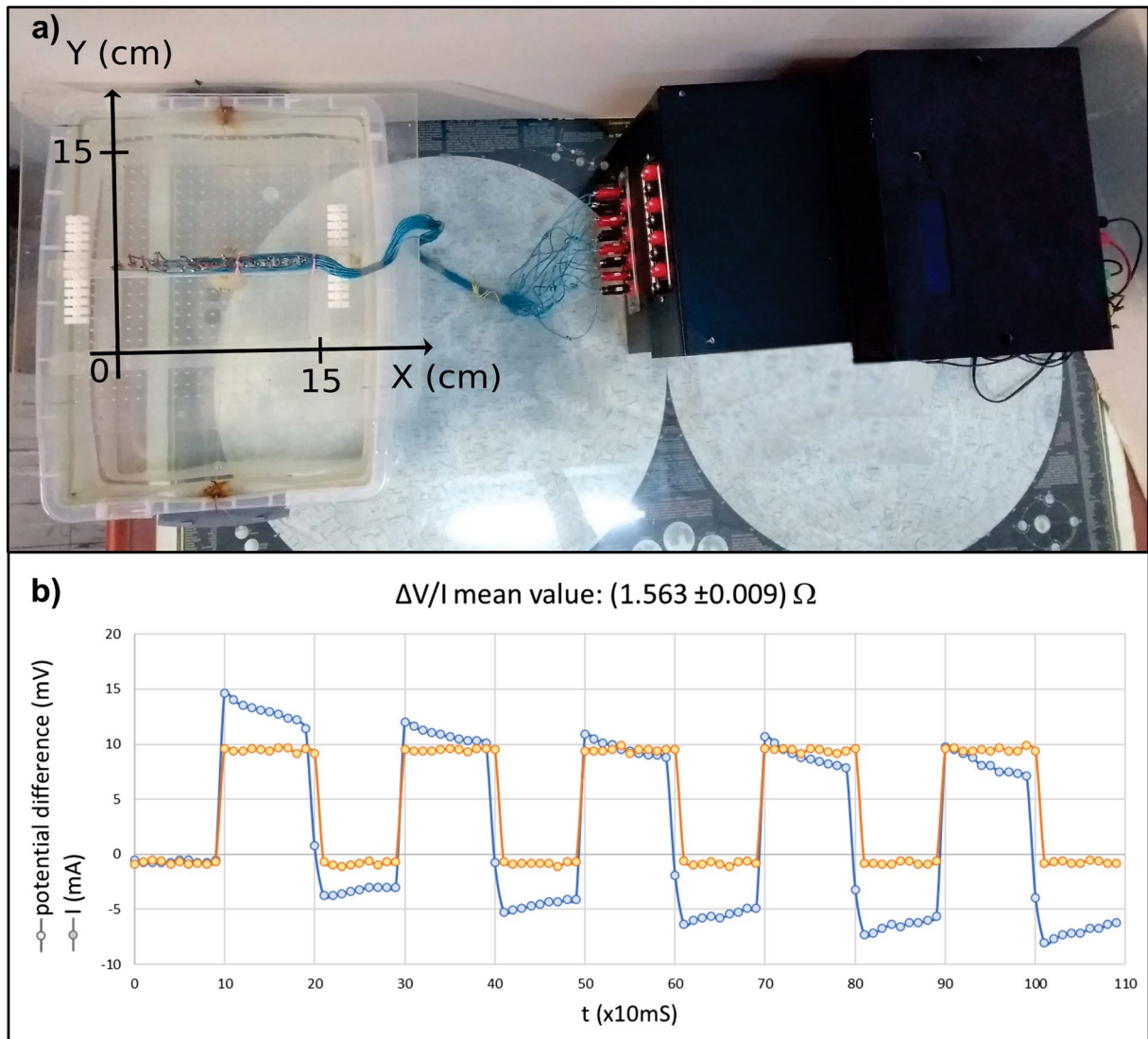


Figure 2. (a) Photo of the physical model and the device prepared for the sphere study. The coordinate system taken in the study area is displayed. (b) Time evolution of signals; potential difference (mV) and I (mA) in the laboratory. A Dipole-Dipole configuration was taken with $a = 1$ cm and $n = 3$.

was inverted using also the Res3DInv code. In Figure 3d the D-D tomography obtained is displayed. The high electrical resistivity ball is perfectly reproduced and the convergence is good (RRMS 4.3%) despite the fact that the resistivity contrast between the ball and the water is not as large as in the previous case.

3.2. Field Study Test

A ERT device testing was performed in a landfill area next to de la Plata River, in Buenos Aires, Argentina. In addition to verify the performance with higher voltages, the localization of the water table was an useful aim, in order to design an additional construction.

A survey line of 7.5 m was performed using the same three programmed configurations than in the previous experiment; D-D, W-S and $W_{Y_{112}}$. The minimum electrode spacing a was set to 0.5 m and the increment displacement was set to 0.5 m. In Figure 4a can be seen a photo of the site with the device connected to the electrodes line prepared for the study.

An input voltage of 50 V and a limiting resistance of 560 ohm was used then a maximum current of 0.09 A is achieved. The time evolution of an individual measurement made on the ground is shown in Figure 4b. A

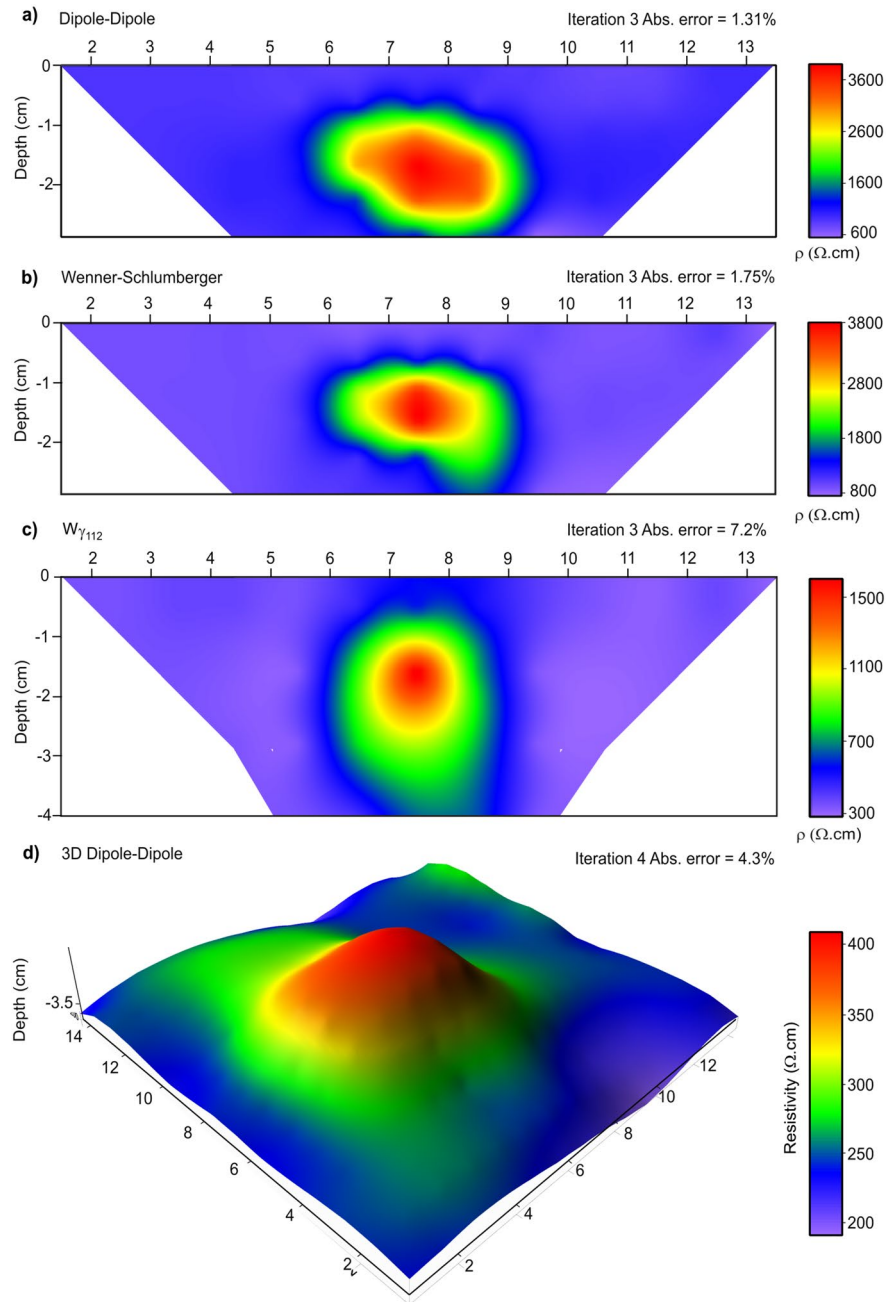


Figure 3. Electrical resistivity tomography (ERT) of the (a) D-D measured data, (b) W-S measured data, (c) $W\gamma_{112}$ measured data and (d) 3D D-D measured data, surface plot at 3.5 cm depth.

Dipole-Dipole configuration was taken with $a = 1\text{ m}$ and $n = 3$. From this graph we obtain a $\Delta V/I$ mean value of 1.053 ohm and a relative standard deviation of 0.8%.

The mean relative standard deviation of the 106 Dipole-Dipole measurements is 5.5%, with a minimum of 0.001% and a maximum of 63.2%. For the 80 Schlumberger-Wenner measurements the values are, mean: 0.6%, minimum: 0.001% and maximum: 1.9%. The values for the 48 $W\gamma_{112}$ and mirror measurements are, mean: 3.1%, minimum: 0.4% and maximum: 34.5%. As in the laboratory case, the highest error of measurements values comes from the furthest potential electrodes. These few points were eliminated before doing the inversion process.

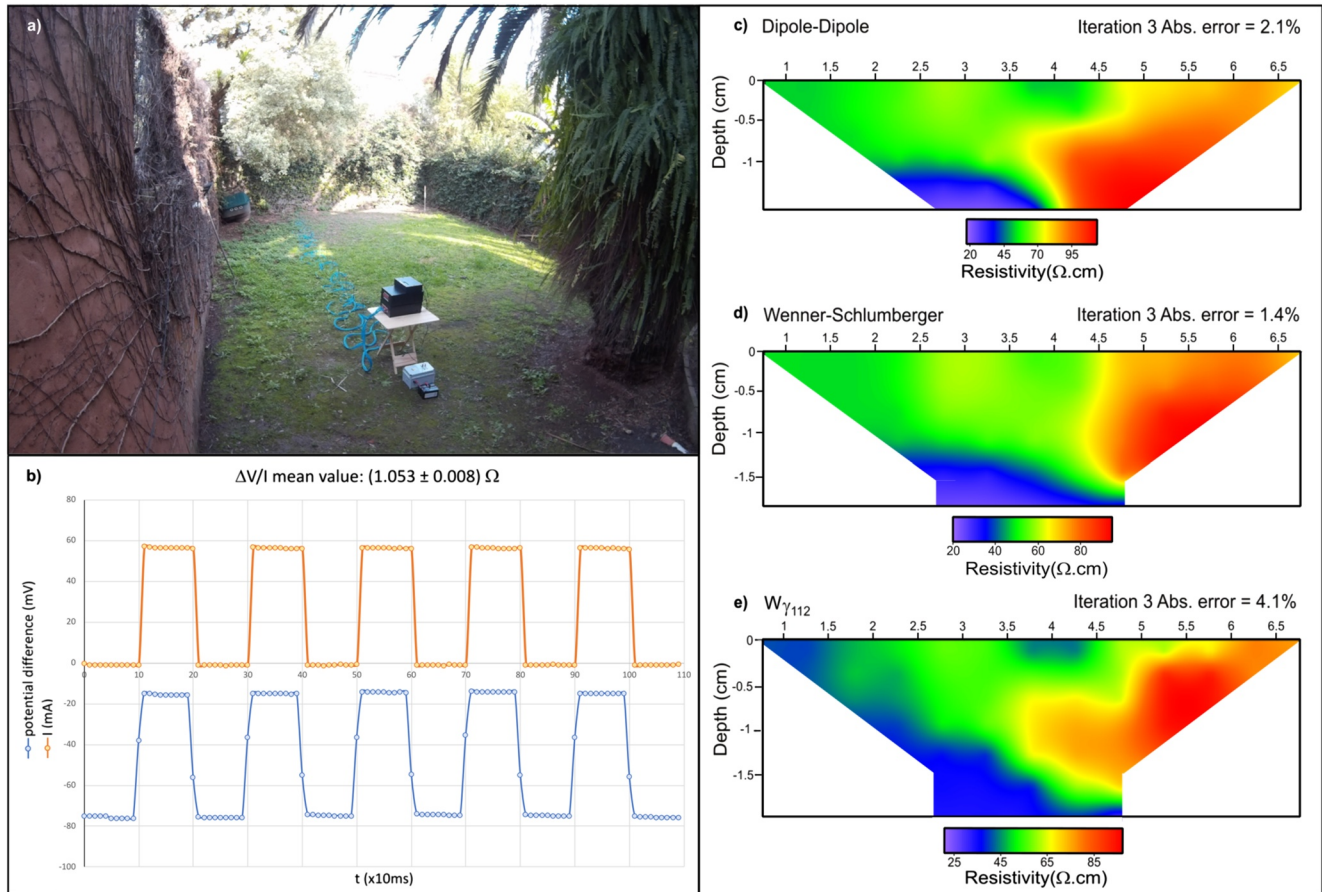


Figure 4. (a) Photo of the testing site. (b) Time evolution of signals; potential difference (mV) and I (mA) in the field. A Dipole-Dipole configuration was taken with $a = 1$ cm and $n = 3$. Inverted ERT cross-sections of the (c) D-D array, (d) W-S array and (e) $W\gamma_{112}$ array.

Figure 4c shows the results of the D-D configuration. A low resistivity anomaly from 2 to 3.5 m below 1 m depth can be distinguished. The RRMS error after the inversion process was 2.1%. Figure 4d shows the results of the W-S configuration. A wider low resistivity anomaly can be distinguished, from 2 to 4.5 m below 1 m. The misfit after the inversion of apparent resistivity data is good (RRMS 1.4%). Figure 4e shows the results of $W\gamma_{112}$ configuration. The convergence is also good (RRMS 4.1%), but in this case, the localization of the anomaly was not so good. In all the cases, the anomaly begins near the origin at lower depth, and ends at higher depth. It can be due to the presence of a tree near the origin of the line, that causes a greater amount of moisture in its vicinity.

4. Conclusions

The individual measurements of voltage and current time evolution performed with the device yielded good results as the standard deviations obtained were small. Furthermore, the measurements were well correlated between them as the inversion tomographies obtained were in agreement with the model.

Regarding the experiment with the ball, the 2D electrical resistivity tomographies obtained in the D-D and W-S and $W\gamma_{112}$ configurations have adequately reproduced the physical model. This shows that the equipment is working properly, with a fine resolution. Especially the $W\gamma_{112}$ configuration can be an efficient tool in order to perform 3D surveys for the detection of localized targets, as it showed a very good resolution with a small amount of measurements compared to traditional configurations. The 3D reconstruction of the ball also shows an excellent agreement with the model. This confirms the good resolution that can be achieved with the device. With respect to the field study, the relative small standard deviations obtained and the good convergence of the inversions denote that the device works properly also in the higher power version. As this device has the possibility to adapt to the needs of the user either by adding modules or by changing the electrode configuration through programming,

we plan to use it to continue research on the presence of tunnels in Parque Avellaneda, an area in the city of Buenos Aires. Future development plans also include both the possibility of using this device in IP studies, as well as adding a module that allows real-time experiments, transferring the data to the web.

Data Availability Statement

The supplemental files may be accessed from a permanent repository at <https://doi.org/10.5281/zenodo.5528209>.

Acknowledgments

This work was partially supported by CONICET (National Scientific and Technical Council Research) and ANP-CyT (National Agency for Scientific and Technological Promotion), Argentina. The authors want to thank Ana Osella and Ernesto López for their assistance in carrying out the construction of the device.

References

- Bergmann, P., Schmidt-Hattenberger, C., Kiessling, D., Rücker, C., Labitzke, T., Hennings, J., et al. (2012). Surface-downhole electrical resistivity tomography applied to monitoring of CO₂ storage at Ketzin, Germany. *Geophysics*, 77(6), B253–B267. <https://doi.org/10.1190/geo2011-0515.1>
- Blackstock, J. M., Covington, M. D., Perme, M., & Myre, J. M. (2019). Monitoring atmospheric, soil, and dissolved CO₂ using a low-cost, Arduino monitoring platform (CO₂-LAMP): Theory, fabrication, and operation. *Frontiers in Earth Science*, 7, 313. <https://doi.org/10.3389/feart.2019.00313>
- Bongiovanni, M., Grünhut, V., Martinelli, P., de La Vega, M., & Bonomo, N. (2018). Geoelectrical and EMI studies at an urban site in Buenos Aires, Argentina, for localizing an old tunnel. *Paper presented at conference and proceedings and 24th European meeting of environmental and engineering geophysics* (pp. 1–5). <https://doi.org/10.3997/2214-4609.201802618>
- Bulgakov, A. Y., & Manshtein, A. K. (2006). A geophysical device for automation of multielectrode electrical prospecting. *Instruments and Experimental Techniques*, 49(4), 565–567. <https://doi.org/10.1134/S002044120604021X>
- Casas, A., Cosentino, P. L., Fiandaca, G., Himi, M., Macias, J. M., Martorana, R., et al. (2018). Non-invasive geophysical surveys in search of the Roman temple of Augustus under the Cathedral of Tarragona (Catalonia, Spain): A case study. *Surveys in Geophysics*, 39(6), 1107–1124. <https://doi.org/10.1007/s10712-018-9470-6>
- Chambers, J., Gunn, D., Wilkinson, P., Meldrum, P., Haslam, E., Holyoake, S., et al. (2014). 4D electrical resistivity tomography monitoring of soil moisture dynamics in an operational railway embankment. *Near Surface Geophysics*, 12, 61–72. <https://doi.org/10.3997/1873-0604.2013002>
- Chambers, J. E., Kuras, O., Meldrum, P. I., Ogilvy, R. D., & Hollands, J. (2006). Electrical resistivity tomography applied to geological, hydrogeological and engineering investigations at a former waste disposal site. *Geophysics*, 71, B231–B239. <https://doi.org/10.1190/1.2360184>
- Chávez, R. E., Cifuentes-Nava, G., Esteban Hernández-Quintero, J., Vargas, D., & Tejero, A. (2014). Special 3D electric resistivity tomography (ERT) array applied to detect buried fractures on urban areas: San Antonio Tecómitl, Milpa Alta, México. *Geofísica Internacional*, 53(4), 425–434. [https://doi.org/10.1016/s0016-7169\(14\)70076-5](https://doi.org/10.1016/s0016-7169(14)70076-5)
- Clément, R., Moreau, S., Henine, H., Guérin, A., Chaumont, C., & Tournebize, J. (2014). On the value of combining surface and cross-borehole ERT measurements to study artificial tile drainage processes. *Near Surface Geophysics*, 12, 2046–2076. <https://doi.org/10.3997/1873-0604.2014034>
- Clément, R., Oxarango, L., & Desclotres, M. (2011). Contribution of 3-D time-lapse ERT to the study of leachate recirculation in a landfill. *Waste Management*, 31, 457–467. <https://doi.org/10.1016/j.wasman.2010.09.005>
- Dahlin, T. (1996). 2D resistivity surveying for environmental and engineering applications. *First Break*, 14(7), 275–283. <https://doi.org/10.3997/1365-2397.1996014>
- de la Vega, M., Bongiovanni, M. V., & Osella, A. (2019). Modular resistivity device for physical model studies. *Paper presented at conference proceedings, 25th European Meeting of Environmental and Engineering Geophysics*. (pp. 1–5). <https://doi.org/10.3997/2214-4609.201902416>
- Eleraki, M., Gadallah, M. M., Gemal, K. S., & Attwa, M. (2010). Application of resistivity method in environmental study of the appearance of soil water in the central part of Tenth of Ramadan City, Egypt. *Quarterly Journal of Engineering Geology and Hydrogeology*, 43(2), 171–184. <https://doi.org/10.1144/1470-9236/08-079>
- Fowler, D. E., & Moysey, S. M. J. (2011). Estimation of aquifer Transport parameters from resistivity monitoring data within a coupled inversion framework. *Journal of Hydrology*, 409, 545–554. <https://doi.org/10.1016/j.jhydrol.2011.08.063>
- Froese, D. G., Smith, D. G., & Clement, D. T. (2005). Characterizing large river history with shallow geophysics: Middle Yukon river, Yukon Territory and Alaska. *Geomorphology*, 67, 391–406. <https://doi.org/10.1016/j.geomorph.2004.11.011>
- Gutiérrez-Martín, A., Yenes, J. I., Fernández-Hernández, M., & Castedo, R. (2021). Stabilization methodology in foundation soils by ERT-3D application in Estepona, South Spain. *Applied Sciences*, 11, 4455. <https://doi.org/10.3390/app11104455>
- Himi, M., Casado, I., Sendros, A., Lovera, R., Rivero, L., & Casas, A. (2018). Assessing preferential seepage and monitoring mortar injection through an earthen dam settled over a gypsiferous substrate using combined geophysical methods. *Engineering Geology*, 246, 212–221. <https://doi.org/10.1016/j.enggeo.2018.10.002>
- Horsburgh, J., Caraballo, J., Ramírez, M., Aufdenkampe, A., Arscott, D., & Damiano, S. (2019). Low-cost, open-source, and low-power: But what to do with the data? *Frontiers in Earth Science*, 7(67), 1–14. <https://doi.org/10.3389/feart.2019.00067>
- Kamiński, M., Zientara, P., & Krawczyk, M. (2021). Electrical resistivity tomography and digital aerial photogrammetry in the research of the “Bachledzki Hill” active landslide – In Podhale (Poland). *Engineering Geology*, 285, 106004. <https://doi.org/10.1016/j.enggeo.2021.106004>
- Kuras, O., Pritchard, J. D., Meldrum, P. I., Chambers, J. E., Wilkinson, P. B., Ogilvy, R. D., et al. (2009). Monitoring hydraulic processes with automated time-lapse electrical resistivity tomography (ALERT). *Comptes Rendus Geoscience*, 341(10–11), 868–885. <https://doi.org/10.1016/j.crte.2009.07.010>
- Kutbay, U., & Hardalaç, F. (2017). Development of a multiprobe electrical resistivity tomography prototype system and robust underground clustering. *Expert Systems*, 34, e12206. <https://doi.org/10.1111/exsy.12206>
- Loke, M. H., & D Barker, R. (1996). RES2DINV and RES3DINV, program distributed by Geotomo, based on rapid least-squares inversion of apparent resistivity pseudosections by a quasi-Newton method. *Geophysical Prospecting*, 44, 499–512. <https://doi.org/10.1111/j.1365-2478.1996.tb00142.x>
- Mao, F., Khamis, K., Krause, S., Clark, J., & Hannah, D. M. (2019). Low-cost environmental sensor networks: Recent advances and future directions. *Frontiers in Earth Science*, 7, 221. <https://doi.org/10.3389/feart.2019.00221>
- Ochs, J., & Klitzsch, N. (2020). Considerations regarding small-scale surface and borehole-to-surface electrical resistivity tomography. *Journal of Applied Geophysics*, 172, 103862. <https://doi.org/10.1016/j.jappgeo.2019.103862>
- Orfanos, C., & Apostolopoulos, G. (2011). 2D–3D resistivity and microgravity measurements for the detection of an ancient tunnel in the Lavrion area, Greece. *Near Surface Geophysics*, 9, 449–457. <https://doi.org/10.3997/1873-0604.2011024>

- Osella, A., Martinelli, P., Grünhut, V., de la Vega, M., Bonomo, N., & Weissel, M. (2015). Electrical imaging for localizing historical tunnels at an urban environment. *Journal of Geophysics and Engineering*, *12*, 674–685. <https://doi.org/10.1088/1742-2132/12/4/674>
- Santarato, G., Ranieri, G., Occhi, M., Morelli, G., Fischanger, F., & Gualerzi, D. (2011). Three-dimensional electrical resistivity tomography to control the injection of expanding resins for the treatment and stabilization of foundation soils. *Engineering Geology*, *119*(1–2), 18–30. <https://doi.org/10.1016/j.enggeo.2011.01.009>
- Saribudak, M., & Van Nieuwenhuise, B. (2006). Integrated geophysical studies over an active growth fault in Houston. *Leading Edge*, *25*(3), 332–334. <https://doi.org/10.1190/1.2184101>
- Sendrós, A., Himi, M., Lovera, R., Rivero, L., Garcia-Artigas, R., Urruela, A., et al. (2020). ERT monitoring of two managed aquifer Recharge ponds in the alluvial aquifer of the Llobregat river (Barcelona, Spain). *Near Surface Geophysics*, *18*, 353–368. <https://doi.org/10.3390/w12123455>
- Simyrdanis, K., Tsourlos, P., Soupios, P., Tsokas, G., Kim, J.-H., & Papadopoulos, N. (2015). Surface-to-tunnel electrical resistance tomography measurements. *Near Surface Geophysics*, *13*, 343–354. <https://doi.org/10.3997/1873-0604.2015019>
- Stummer, P., Maurer, H., & Green, A. G. (2004). Experimental design: Electrical resistivity data sets that provide optimum subsurface information. *Geophysics*, *69*, 120–139. <https://doi.org/10.1190/1.1649381>
- Stummer, P., Maurer, H., Horstmeyer, H., & Green, A. G. (2002). Optimization of dc resistivity data acquisition: Real-time experimental design and a new multielectrode system. *IEEE Transactions on Geoscience and Remote Sensing*, *40*(12), 2727–2735. <https://doi.org/10.1109/TGRS.2002.807015>
- Szalai, S., Lemperger, I., Metwaly, M., Kis, A., Westergom, V., Szolokili, V., et al. (2015). Increasing the effectiveness of electrical resistivity tomography using γ_{11n} configurations. *Geophysical Prospecting*, *63*, 508–524. <https://doi.org/10.1111/1365-2478.12215>
- Tejero-Andrade, A., Argote-Espino, D. L., Cifuentes-Nava, G., Hernández-Quintero, E., Chávez, R. E. Y., & García-Serrano, A. (2018). ‘Illuminating’ the interior of Kukulcan’s Pyramid, Chichén Itzá, Mexico, by means of a non-conventional ERT geophysical survey. *Journal of Archaeological Science*, *90*, 1–11. <https://doi.org/10.1016/j.jas.2017.12.006>
- Tsokas, G. N., Tsoulos, P. I., Vargemesis, G., & Pazaras, N. (2011). Using surface and cross-hole resistivity tomography in an urban environment: An example of imaging the foundations of the ancient wall in Thessaloniki, North Greece. *Physics and Chemistry of the Earth*, *36*, 1310–1317. <https://doi.org/10.1016/j.pce.2011.03.007>
- Tziortzioti, C., Amaxilatis, D., Mavrommati, I., & Chatzigiannakis, I. (2019). IoT sensors in sea water environment: Ahoy! experiences from a short summer trial. *Electronic Notes in Theoretical Computer Science*, *343*, 117–130. <https://doi.org/10.1016/j.entcs.2019.04.014>
- Vaudelet, P., Schmutz, M., Pessel, M., FranceschiGuérin, M., Atteia, O., Blondel, A., et al. (2011). Mapping of contaminant plumes with geoelectrical methods. A case study in urban context. *Journal of Applied Geophysics*, *75*(4), 738–751. <https://doi.org/10.1016/j.jappgeo.2011.09.023>
- Wilkinson, P. B., Chambers, J. E., Uhlemann, S., Meldrum, P. I., Smith, A., Dixon, N., et al. (2016). Reconstruction of landslide movements by inversion of 4-D electrical resistivity tomography monitoring data. *Geophysical Research Letters*, *43*, 1166–1174. <https://doi.org/10.1002/2015GL067494>
- Wilkinson, P. B., Meldrum, P. I., Chambers, J. E., Kuras, O., & Ogilvy, R. D. (2006). Improved strategies for the automatic selection of optimized sets of electrical resistivity tomography measurement configurations. *Geophysical Journal International*, *167*(33), 1119–1126. <https://doi.org/10.1111/j.1365-246X.2006.03196.x>
- Yeh, H. F., Lin, H. I., Wu, C. S., Hsu, K. C., Lee, J. W., & Lee, C. H. (2015). Electrical resistivity tomography applied to groundwater aquifer at downstream of Chih-Ben Creek basin, Taiwan. *Environmental Earth Sciences*, *73*, 4681–4687. <https://doi.org/10.1007/s12665-014-3752-1>
- Zhe, J., Greenhaigh, S., & Marescot, L. (2007). Multichannel, full waveform and flexible electrode combination resistivity-imaging system. *Geophysics*, *72*(2), F57–F64. <https://doi.org/10.1190/1.2435081>